Journal of Bionic Engineering (2022) 19:1392–1404
https://doi.org/10.1007/s42235-022-00205-0

RESEARCH ARTICLE

Design and Analysis of a 2-DOF Actuator with Variable Stiffness Based on Leaf Springs

ShangKui Yang[1,2,3] · Peng Chen[1,2,4] · DongQi Wang[1,2] · Yi Yu[1,2,4] · YuWang Liu[1,2]

Received: 4 January 2022 / Revised: 9 April 2022 / Accepted: 13 April 2022 / Published online: 11 May 2022

Abstract
Variable Stiffness Actuator (VSA) is the core mechanism to achieve physical human–robot interaction, which is an inevitable development trend in robotic. The existing variable stiffness actuators are basically single degree-of-freedom (DOF) rotating joints, which are achieving multi-DOF motion by cascades and resulting in complex robot body structures. In this paper, an integrated 2-DOF actuator with variable stiffness is proposed, which could be used for bionic wrist joints or shoulder joints. The 2-DOF motion is coupling in one universal joint, which is different from the way of single DOF actuators cascade. Based on the 2-DOF orthogonal motion generated by the spherical wrist parallel mechanism, the stiffness could be adjusted by varying the effective length of the springs, which is uniformly distributed in the variable stiffness unit. The variable stiffness principle, the model design, and theoretical analysis of the VSA are discussed in this work. The independence of adjusting the equilibrium position and stiffness of the actuator is validated by experiments. The results show that the measured actuator characteristics are sufficiently matched the theoretical values. In the future, VSA could be used in biped robot or robotic arm, ensuring the safety of human–robot interaction.

Keywords Physical human–robot interaction · 2-DOF · Bionic wrist joints · Variable stiffness actuator · Leaf spring

1 Introduction

With the development of cooperative robots, robots are no longer confined to traditional industrial production in structured environment, but gradually going to unstructured environments for physical Human–Robot Interaction (pHRI). Complying with the core criterion of safety for pHRI, the robot should not be dangerous for operators, which requires future robots with abilities of variable stiffness and compliant as humans.

To improve the safety of the robot, the best option is to mimic the stiffness adjustment of the human arm joints [1, 2]. Based on the bionic principle of human muscles, early researchers proposed the pneumatic and electrical polymer artificial muscles [3]. Meanwhile, researchers have added elastic elements between the traditional actuator and the load to form a Series Elastic Actuator (SEA), which achieves flexibility and safety [4]. However, the applications of artificial muscles and SEA are limited owing to their non-adjustable stiffness. Different from the fixed compliance type joint, the stiffness of the actuator could be changed dynamically, which could maximize storage and release the impact energy, ensuring the safety of pHRI [5].

The stiffness of biological joints could be adjusted through the joint contraction of agonist and antagonist, which has been applied in robot technology [6]. In this way, based on the antagonism principle of human arm muscles, where two elastic components work together to control the equilibrium position of the joints and generate compliant torque, two motors are used to adjust the antagonistic. Antagonistic VSAs are mainly divided into two types: series [7] and parallel [8]. The VSA-I and VSA-II prototype are examples of the antagonism principle [9, 10]. However,

✉ YuWang Liu
liuyuwang@sia.cn

1 State Key Laboratory of Robotics, Shenyang Institute of Automation, Chinese Academy of Sciences, Shenyang 110000, China

2 Institutes for Robotics and Intelligent Manufacturing, Chinese Academy of Sciences, Shenyang 110000, China

3 Key Laboratory of Mechanism Theory and Equipment Design of Ministry of Education School of Mechanical Engineering, Tianjin University, Tianjin 300192, China

4 University of Chinese Academy of Sciences, Beijing 100049, China

the synchronous control method, which causes high energy consumption and control complexity, seriously limited the applications of antagonistic VSA.

In contrast to the previous concept of antagonistic control of stiffness, mechanical structural control could achieve changing stiffness by adjusting the effective length of spring where AwAs-I [11], AwAs-II [12], compact-VSA [13], and HVSA [14] are representative examples. The mechanical structure of VSA used the position motor to increase the mechanical adaptability, and used the stiffness motor to change the strain of elastic element or the effective length of lever for variable stiffness performance. This method can quickly adjust the joint stiffness and reduce the energy loss. Currently, this type of variable stiffness joints generally used ball screws, racks, or planetary gear trains to change the position of the fulcrum, which caused the larger structure.

In addition, Groothuis et al. [15] and Wolf et al. [16] used the principle of cantilever beams to achieve stiffness adjustments by changing the effective lengths of elastic elements. Although the position and stiffness can be controlled independently, but the two actuators must always operate synchronously, which would cause the controller extremely complex and low space utilization. Fortunately, the simplified design of the variable stiffness joints and commercial off-the-shelf components provided an opportunity to reduce the cost by reducing the number of custom-made parts [5].

To summarize, the various VSAs, with functions of imitating human work behavior, are designed to refer human structures [17, 18], which is a typical ball socket joint driven by parallel muscle clusters [19], as shown in Fig. 1. However, the current studies are mainly focused on 1-DOF variable stiffness joints, lacking studies on multi-DOF variable stiffness joints [20].

With the aim of resolving such problems, a novel compact structure and small volume 2-DOF VSA for shoulder joint applications is proposed, and the stiffness could be adjusted by changing the effective length of the leaf springs. The 2-DOF motion is achieved by a Spherical Wrist Parallel Mechanism (SWPM), which acts like a universal joint (U-joint). Therefore, the SWPM can imitate the movement of the human shoulder joints. The leaf springs are arranged in parallel, which significantly reduces the mass and volume of the actuators. The mathematical model is developed to reveal workspace and variable stiffness performance. The characterization of the actuator is experimentally tested and verified.

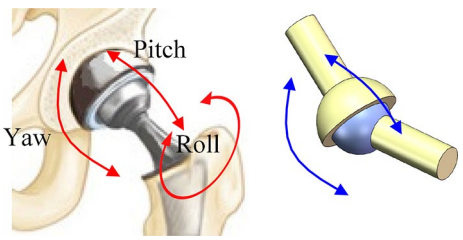

Fig. 1 Structure of human ball-and-socket joint

The organization of this paper is as follows: In Sect. 2, the method and principle of variable stiffness are introduced. In Sect. 3, the modeling of a 2-DOF VSA is described, and the analysis and calculation of the actuator are given. In Sect. 4, the prototype, related experiments, and a comparative analysis are described. Finally, future work and concluding remarks are given in Sects. 5 and 6.

2 Mechanical Design

2.1 Principle of the 2-DOF VSA

The conceptual design of 2-DOF VSA is shown in Fig. 2. Based on the structure of human shoulder joint (a), the form of a spherical wrist joint is proposed to realize a 2-DOF VSA (b). The rod at the top of the actuator acts as power output. The screw is driven by adjusting motor to change the slider position on leaf spring, thereby adjusting the stiffness of actuator. The rotation 1 and rotation 2 are connected by a coupling device, and be driven to deflect through the output rod. The workspace of the output rod is a sphere, which can successfully imitate the front–back and left–right movement of the human shoulder joint.

2.2 Variable Stiffness Mechanism Based on Leaf Springs

The structure of VSA adopts a parallel and uniform arrangement of the leaf springs, as shown in Fig. 3a. The rollers could be driven simultaneously by a single motor, and moving parallel along the leaf springs. The 2-DOF VSA adjusts the stiffness of the joint by changing the elastic deformation ability of the leaf springs, as shown in Fig. 3b. When the rotating shaft rotates around its center, the free end of the leaf springs deflects with the lever arm on the rotating shaft, where the part of the leaf springs between the guide rail and roller will be deformed. When the actuator is operating, the direction of the deflections of the leaf spring is perpendicular to the load direction caused by the elastic elements, which means that the load is perpendicular to the force of the stiffness adjustment. By changing the distance between the guide rail and the roller to change the effective length of the leaf springs, so as to achieve active control of the stiffness.

The SWPM is used to achieve a 2-DOF U-joint motion. The structure can operate as a human shoulder joint. The SWPM consists of four parts: rotating shaft 1, rotating shaft 2, parallel mechanism 1, and parallel mechanism 2.

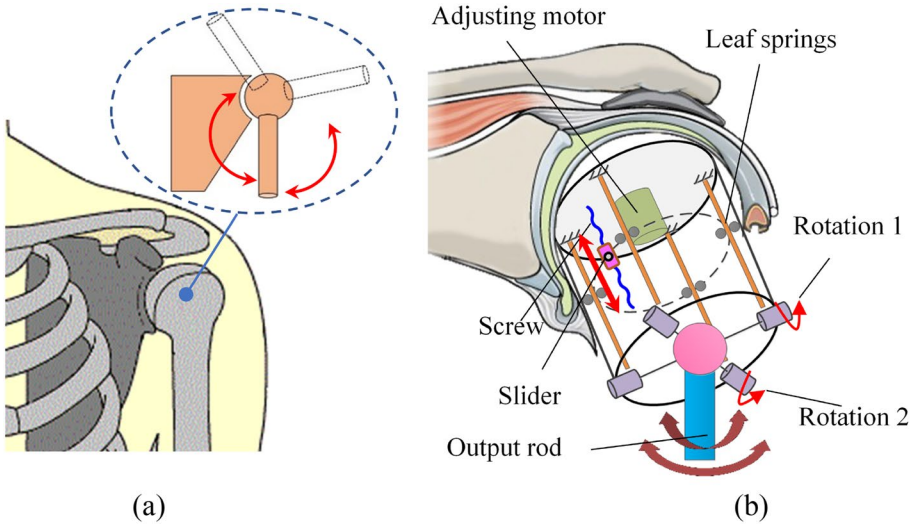

Fig. 2 Conceptual design of 2-DOF VSA. **a** Front-back and left–right movement of human shoulder joint. **b** 2-DOF VSA is designed to imitate human shoulder joint

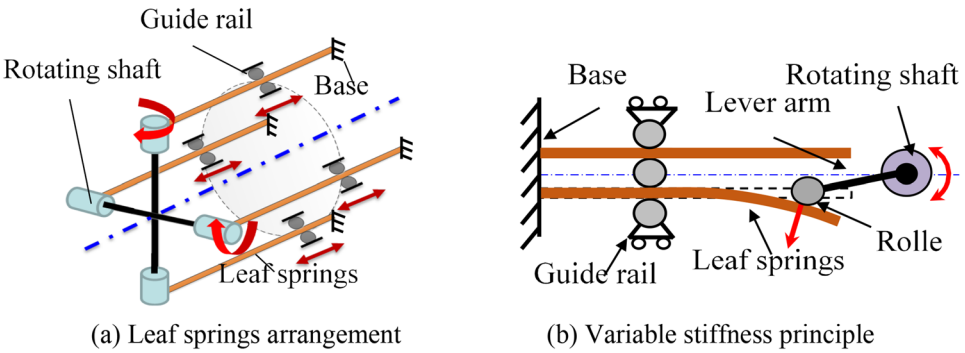

Fig. 3 Variable stiffness unit of the 2-DOF VSA

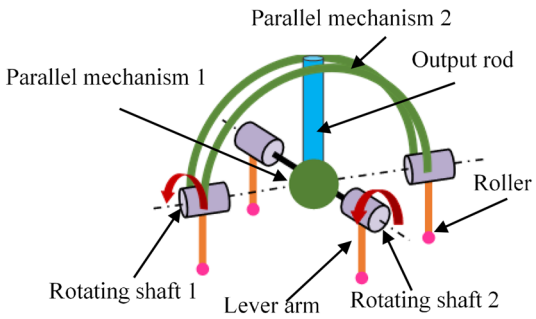

Fig. 4 Principle of 2-DOF SWPM

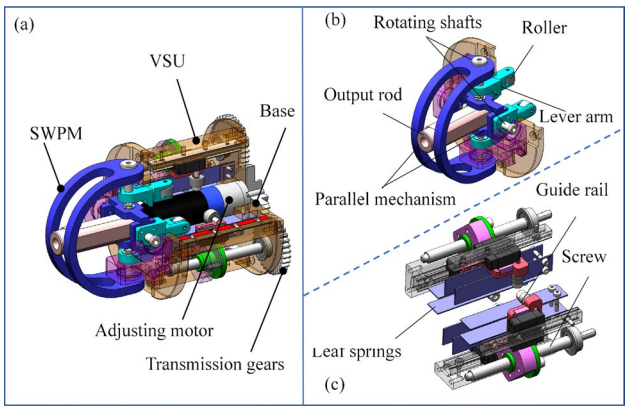

Fig. 5 CAD model of 2-DOF VSA: **a** detailed implementation of 2-DOF VSA, **b** SWPM, and **c** VSU

These four parts are each connected by an output rod, and the rods intersect at the center of the actuator. The rotating shafts are coupled by parallel mechanisms and output rod, as shown in Fig. 4. When the output rod is deflected, the rotating shafts rotate simultaneously due to the coupling effect of the parallel mechanisms. The rollers are connected to the lever arm and interact with the free end of the leaf springs, as shown in Fig. 3.

2.3 Mechanical Design of the Actuator

As shown in Fig. 5a, a detailed implementation scheme of a 2-DOF VSA was designed. The 2-DOF VSA consists of two parts: an SWPM and a Variable Stiffness Unit (VSU), shown in Fig. 5b, c. The leaf springs are arranged orthogonally

and connected to the rotating shafts of parallel mechanisms. The four rollers are torque-generating elements that act in contact with the free ends of the leaf springs in each direction, respectively, resulting in an anti-torque effect. When the 2-DOF VSA output rod is in an equilibrium position and the adjustment slider is at the end of the guide rail, there is no force on either side of the roller. All leaf springs are in a natural state, and the 2-DOF VSA is in a maximum state of compliance. A motor is fixed in the center of the base and the adjusting the rollers move parallel along the leaf springs. It mainly adjusts the effective length of the VSU leaf springs synchronously to achieve a continuous stiffness adjustment. When the adjusting motor changes the distance of the adjustment slider to control the distance between the guide rail and the roller (the effective length of the leaf springs), the resistance torque of the leaf springs increases (or decreases), which causes the output stiffness to change as the slider moves.

3 Modeling of the 2-DOF VSA

The stiffness adjustment of the 2-DOF VSA is realized through adjusting the effective length of leaf springs. L is the effective length of the leaf springs during the movement of the guide rail. θ is the deflection angle of the leaf springs. ω_1 is the deflection of the end of the leaf springs under the load. The principle of the VSU is shown in Fig. 6, where $\boldsymbol{M}$ is the component torque of the actuator, $\boldsymbol{F}$ represents the force between the roller and leaf springs, and φ represents the deflection angle of the output end with respect to the equilibrium position. Joint axis point o denotes the axis of the output joint, around which the output part of the joint with variable stiffness will rotate.

According to the geometric relation shown in Fig. 6, the force $\boldsymbol{F}$ is acting on the leaf springs in the point Q_i, which is the end point for the point Q_0 moving on the arch. R is the distance between the center point of the roller and the center point o of the output joint. The roller has a radius of r. The vertical displacement distance of roller center is ω_1:

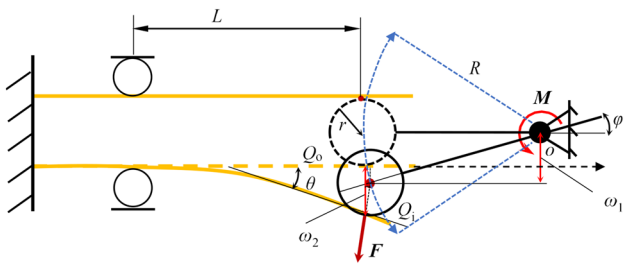

Fig. 6 Modeling and analysis of the VSU. Computational model of the variable stiffness

$$R\sin\varphi = \omega_1. \tag{1}$$

When the actuator outputs the torque, the force direction of the free end of the leaf springs will change, and the force direction will follow the leaf springs bending perpendicular to the surface. The Q_i point deflection and angle can be obtained:

$$\omega_2 = \frac{\boldsymbol{F}L^3}{3EI}, \tag{2}$$

$$\theta = \frac{\boldsymbol{F}L^2}{2EI}. \tag{3}$$

Because the deflection angle of the leaf spring is less, $\cos\theta$ is approximately equal to 1:

$$\omega_2 = R\sin\varphi + r(\cos\theta - 1). \tag{4}$$

The free end deflection ω_2 of the leaf spring is approximately equal to the vertical moving distance ω_1 of the roller center:

$$\omega_2 = \omega_1. \tag{5}$$

The load on the free end is

$$\boldsymbol{F} = \frac{3\sin\varphi EIR}{L^3}. \tag{6}$$

The cross-sectional area of the leaf springs is rectangular, and its cross-section moment of inertia is

$$I = \frac{ab^3}{12}. \tag{7}$$

The a is the length of the rectangular cross-section of the leaf springs, and the b is the width of the rectangular cross-section of the leaf springs.

There is a very important relationship between the angle φ of VSA and the deflection angle θ of leaf springs, in the determination of actuator size, torque size, and stiffness range analysis. According to the deflection angle Eqs. (2) and (3) of the free end and the vertical displacement distance of roller center is ω_1 and Eq. (5), the relationship between the passive deflection angle and the bending angle of the VSA can be obtained $\varphi_{\max}$:

$$\varphi_{\max} = \arcsin\left(\frac{2L}{3R}\tan\theta_{\max}\right). \tag{8}$$

In this study, the core element of the VSA is the leaf springs. The reliability analysis of the leaf springs ensures that the elastic element does not produce plastic deformation in the maximum bending. The limit deflection angle θ of the leaf springs is limited to less than 12°. The small deflection of the beam is the main one, and the

approximate differential equation of the deflection of the beam is used. To make the VSA meet the design requirements, its stiffness characteristics and maximum torque value are within the safe range.

When the passive angle of the VSA reaches maximum, the bending angle of the leaf springs also reaches the maximum value. The bending moment of the leaf springs clamped on the roller is the maximum, and the bending normal stress is

$$\begin{cases} \sigma_{\max} = \frac{M_z}{W_z} \\ W_z = \frac{ab^2}{6} \\ M_z = FL \end{cases}. \tag{9}$$

The above conditions are brought into Eq. (5) to obtain the maximum bending normal stress on the leaf springs for

$$\sigma_{\max} = \frac{6FL}{ab^2}. \tag{10}$$

To ensure that the variable stiffness actuator is in the reliable range. It is necessary to ensure that the core element leaf spring does not produce bending deformation, and its maximum bending is within the allowable tensile stress range:

$$\sigma_{\max} \le [\sigma] = \frac{\sigma_s}{n}. \tag{11}$$

For plastic materials, the tensile stress is σ_s/n, where n is the safety factor.

The following load $\boldsymbol{F}$ Eq. (6) on the free end of the leaf spring is substituted into the Eqs. (10) and (11), and the effective length L range Eq. (7) of the leaf spring is obtained

$$L \ge \frac{nEb\tan\theta}{\sigma_s}. \tag{12}$$

Leaf springs of 65 Mn are adopted for the actuator. Its cross-section is $a = 10$ mm, $b = 0.6$ mm, its elastic modulus is $E = 208$ Gpa, and its yield strength is $\sigma_s = 726$ MPa. Based on the small deformation theory of cantilever beam, the deflection angle of leaf springs is $\theta = 12°$, and the integral value is $L = 45$ mm.

Take L into Eq. (12) to obtain the deflection angle of the actual leaf springs $\theta = 12.04°$. Deflection angle $\varphi_{\max} = 14.83°$. Substituting $L = 45$ mm, its lever arm length is $R = 25$ mm, its roller radius is $r = 5$ mm to Eq. (8), and the limit deflection angle of variable stiffness actuator $\varphi_{\max} = 14.83°$ is obtained.

A curve of the passive deflection limit $\varphi_{\max}$ as a function of the effective length L of the leaf spring can be made from Eq. (8). As the effective length of the leaf spring increases, the passive deflection angle of the output rod increases approximately linearly.

Torque of the force $\boldsymbol{F}$ acting on rollers

$$\boldsymbol{M} = \boldsymbol{F}(R\cos\varphi - r\sin\varphi). \tag{13}$$

Substituting Eq. (6) into the Eq. (13) can be obtained

$$\boldsymbol{M} = \frac{3R\sin\varphi EI(R\cos\varphi - r\sin\varphi)}{L^3}. \tag{14}$$

Furthermore, the stiffness of the 2-DOF VSA is obtained by combining Eqs. (14) and (15):

$$K = \frac{\mathrm{d}\boldsymbol{M}}{\mathrm{d}\varphi}, \tag{15}$$

$$K = \frac{3EI(R^2\cos(2\varphi) - Rr\sin(2\varphi))}{L^3}. \tag{16}$$

According to Eq. (14), the relationship between the passive angle and the effective length is shown in Fig. 7. When the physical properties of the leaf springs are determined, the effective length of the leaf springs and the passive deflection angle φ changing the torque of the actuator can also be determined. It can be seen that the torque of the 2-DOF VSA increases nonlinearly when the effective length of the leaf springs decreases, and the torque reaches the maximum when $L = 0$. The maximum torque of the actuator is 60 N·m, which depends on the leaf springs within the yield range.

To obtain an accurate output of the coupling torque and a coupling stiffness of the output rod, a theoretical analysis of the SWPM is carried out. The torque model is set in spherical coordinates, and the workspace of the output rod is spherical. The origin is set at the orthogonal position of the rollers. As shown in Fig. 8a, α is the rotational angle component of the

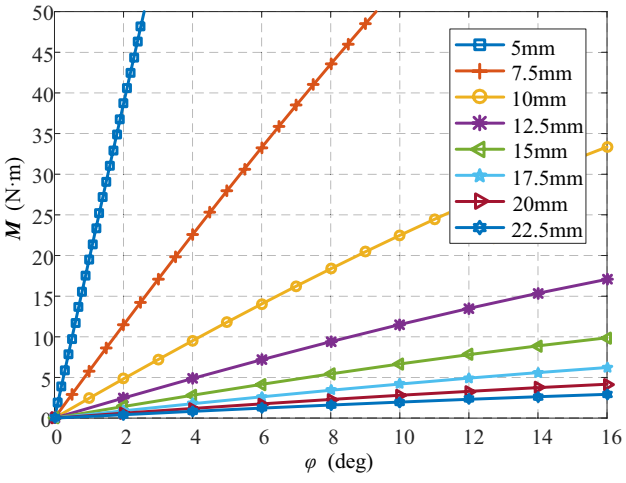

Fig. 7 Theoretical analysis of variable stiffness characteristics. Torque curve of the actuator with different effective lengths

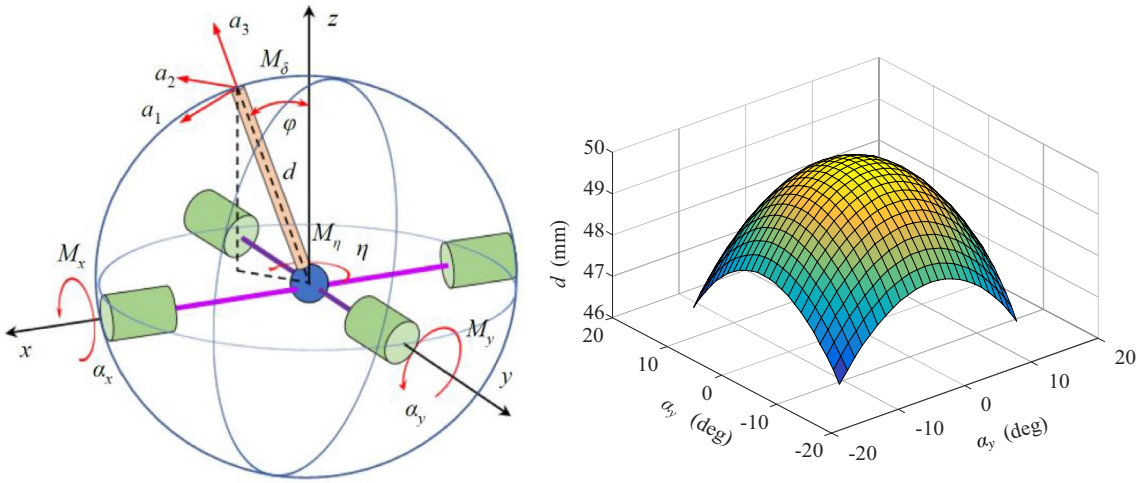

(a) Static analysis of SWPM.

(b) Output workspace of SWPM.

Fig. 8 Analysis of SWPM

SWPM, δ and η are the rotation angles of the horizontal and vertical planes respectively in the spherical coordinates, M_δ and M_η is the component of the torque $\boldsymbol{M}$ in different directions, and d is the radius of the output rod. The length of the output rod is 50 mm, and its working surface is a part of the spherical surface. The spherical vertex in Fig. 8b shows the position of the output rod under no load. The α_x and α_y angles represent the position of the output rod in when the maximum rotation angle φ of the two rollers are $\pm 14.83°$.

The $\boldsymbol{a}$ is the coordinate at the top of the output rod. The workspace of SWPM is given by

$$\boldsymbol{a}_3 = \boldsymbol{a}_1 \times \boldsymbol{a}_2 = \frac{\cos\alpha_x \sin\alpha_y}{\sqrt{1-\sin^2\alpha_x \sin^2\alpha_y}}\boldsymbol{i} - \frac{\sin\alpha_x \cos\alpha_y}{\sqrt{1-\sin^2\alpha_x \sin^2\alpha_y}}\boldsymbol{j} + \frac{\cos\alpha_x \sin\alpha_y}{\sqrt{1-\sin^2\alpha_x \sin^2\alpha_y}}\boldsymbol{k}. \tag{17}$$

The relationship between the coordinate of SWPM and the rotational angle of the rotation axis is as follows:

$$\begin{cases} \eta = \arctan\left(\dfrac{\alpha_x}{\alpha_y}\right) \\ \delta = \sqrt{\alpha_x^2 + \alpha_y^2} \end{cases}. \tag{18}$$

For the rigidity of the SWPM and constant speed, the differential matrix of the angle of Eq. (18) is shown through Eq. (19), and the speed of the SWPM and the speed of the rollers are coupled by a constant linear relationship $\boldsymbol{J}$:

$$\begin{bmatrix} \mathrm{d}\eta \\ \mathrm{d}\delta \end{bmatrix} = \boldsymbol{J}\begin{bmatrix} \mathrm{d}\alpha_x \\ \mathrm{d}\alpha_y \end{bmatrix}, \tag{19}$$

$$\boldsymbol{J} = \begin{bmatrix} \dfrac{\alpha_y}{\alpha_x^2+\alpha_y^2} & -\dfrac{\alpha_x}{\alpha_x^2+\alpha_y^2} \\ \dfrac{\alpha_x}{\sqrt{\alpha_x^2+\alpha_y^2}} & \dfrac{\alpha_y}{\sqrt{\alpha_x^2+\alpha_y^2}} \end{bmatrix}. \tag{20}$$

The output torque $\boldsymbol{M}_\mathrm{o}$ relationship can be obtained as follows:

$$\boldsymbol{M}_\mathrm{o} = \boldsymbol{J}^\mathrm{T}\boldsymbol{M}. \tag{21}$$

It can be seen from Fig. 8 that the coupling matrix $\boldsymbol{J}$ indicates that the SWPM is affected by the two directions of the motions, and the placement stiffness of the roller is $k_1 = k_1(L)$ and $k_2 = k_2(L)$. The VSA with a coupling stiffness output K_o are given by the following:

$$K_\mathrm{o} = \boldsymbol{J}^{-\mathrm{T}}\begin{bmatrix} k_1 & 0 \\ 0 & k_2 \end{bmatrix}\boldsymbol{J}^{-1}. \tag{22}$$

4 Experiments and Results

4.1 Experimental Prototype

The experimental platform of the VSA consists of the position drive motor, the control board, and the encoder, as shown in Fig. 9. The angle of rotation of the joints is measured by the encoder. When the adjustment motor rotates, it

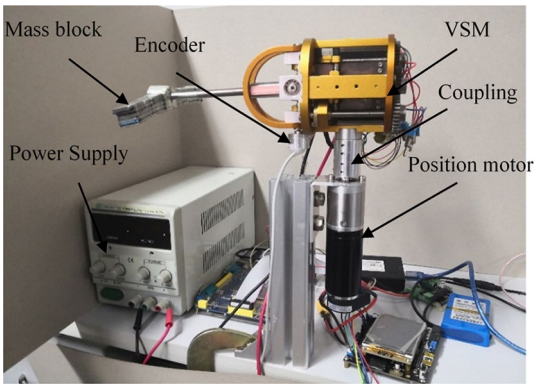

Fig. 9 2-DOF VSA experiment platform

drives the screw to rotate and adjust the effective length of the leaf springs.

4.2 Actual Output Torque Measurement

To verify the variable stiffness characteristics of the 2-DOF VSA, the actual stiffness of the VSA is obtained. The curve of the passive deflection angle φ and the torque $\boldsymbol{M}$ is obtained by applying a static load to the VSA. To quantify the effect of the effective length of the leaf springs on the VSA stiffness, the following experiments were carried out on a VSU with 6 effective length L (ranging from 10 to 35 mm with increments of 5 mm) springs. Based on the experimental data-point fitting, the relationship between the deflection angle and the torque of the 2-DOF VSA is as shown in Fig. 10a. Through comparison, it is found that there are errors between the theoretical value and the experimental value. The main reason is that the gravity effect of the output rod and the measurement error are not ignored. The torque–deflection angle curve of the loading and unloading phases is shown in Fig. 10b. During the unloading phase, a torque hysteresis exists. The hysteresis is larger in the lower stiffness presets, and smaller in the higher presets. The hysteresis in the lower stiffness presets is mainly caused by the machining error of the joint and the internal friction and clearance. In the high preset, the stiffness hysteresis is small, mainly owing to the elastic deformation of the leaf springs.

4.3 Regulation Response

This experiment was conducted to obtain the static stiffness of the VSA by applying an increasing static load to the VSA to obtain the relationship between the passive deflection angle of the actuator and the load moment. The base was controlled to move from the initial position point ($L = 35$ mm) by a single movement of 5 mm, and at each position point, the loading conditions were varied, and the magnitude of the static moment and the passive deflection angle of the output rod were recorded. The comparison between theoretical stiffness and measured stiffness of 2-DOF VSA is shown in Fig. 11a. It can be seen that the actual stiffness is below the theoretical stiffness. This is due to the gap between the machining error and the mechanical structure. The time required for a minimum to maximum stiffness adjustment is measured by the adjusting motor, as shown in Fig. 11b. During the experiment, a load of 286.7 g is applied at the end of the output rod. The rollers moved rapidly from 35 to 10 mm in terms of the effective length,

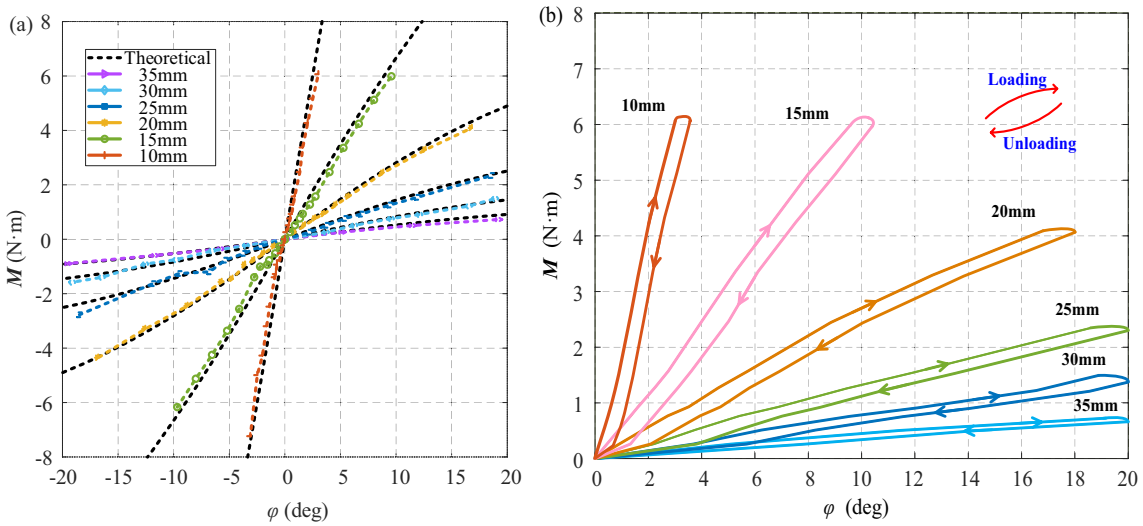

Fig. 10 Torque versus deflection by static experiments of VSA with different rotation angles. **a** Stiffness profile of 2-DOF VSA with regulating displacement 10–35 mm. **b** The torque–deflection angle curve of the loading and unloading phases

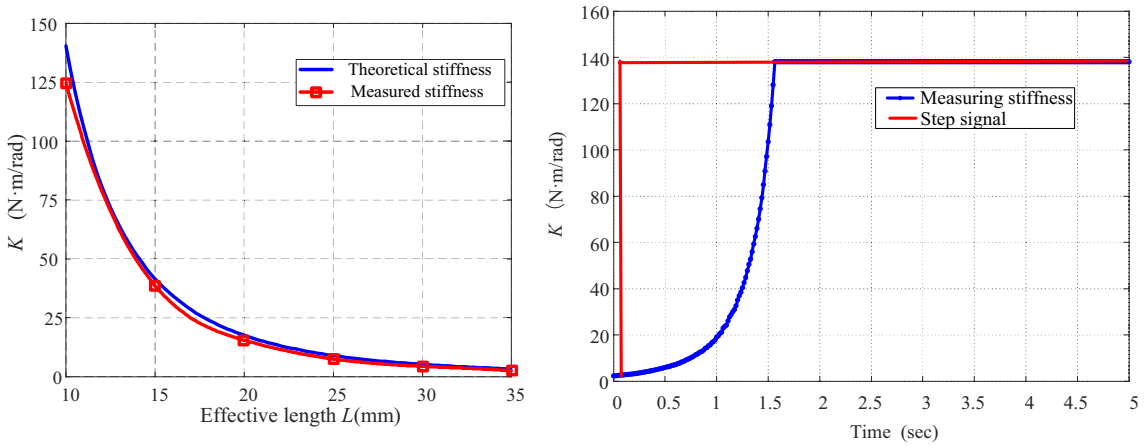

Fig. 11 Variable stiffness analysis of the 2-DOF VSA. **a** Theoretical stiffness and measurement stiffness. **b** Stiffness step response experiment

and the stiffness changes from 2.38 to 138.17 N·m/rad in 1.5 s.

4.4 Tracking Results

The position tracking experiment verifies the oscillatory characteristics of the end of the actuator. The deviation between the expected position and the actual position of the motor is reduced by the PD controller, and the semi-closed-loop tracking control of the stiffness is finally completed. The output rod (rod length 100 mm, weight 32 g) was first placed in the equilibrium position without load. The guide rails were moved to 10 mm (high stiffness = 125 N m/rad) and 35 mm (low stiffness = 2.5 N m/rad) for comparison experiments. The driving position motor of the joint rotates the joint from the equilibrium position to 120°. The rotation speed is 6.46 rad/s. The encoder readings were recorded at 0.02 s intervals and the motor position was plotted against the experimental data as a function of time. It can be seen from Fig. 12 that the smaller the stiffness is, the larger the amplitude of the vibration. The rise time is 0.103 s under high stiffness with a settling time of 0.297 s. The rise time is 0.196 s under low stiffness with a settling time of 0.804 s. The position tracking experiment verified that the joint has good stiffness and positional accuracy when moving.

The 2-DOF VSA has to have a high bandwidth performance to ensure that the actuator can deliver the required torque/position accurately and quickly. In the process, the actuator has to ensure a stable response to reduce oscillations and improve the smoothness and safety of the interaction.

Experiments on position tracking of the VSA at low and high loads (low load = 5 g, high load = 500 g) with $K_1 = 2.5$ N m/rad and $K_2 = 100$ N m/rad stiffness. As can be seen in Fig. 13a, b, the position output curve matches the reference signal better at high stiffness and low load, and the overall position response of the VSA is more

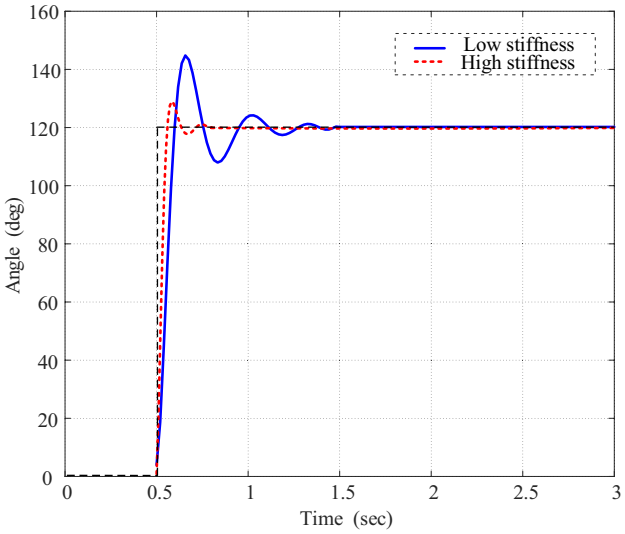

Fig. 12 Position tracking experiment

accurate. The VSA was given a constant load of 0.5 N m during motion at low stiffness (2.5 N m/rad) and the test results are shown in Fig. 13c. The same control conditions were then maintained and the applied load was changed to 15 N m to evaluate the torque tracking performance of the VSA at high stiffness (100 N m/rad) and the results are shown in Fig. 13d.

When the applied load was 1.5 N m, the VSA oscillated slightly in response, producing a maximum overshoot of 0.19 N m, indicating a maximum tracking error of 12.7% during actuator tracking of a 1.5 N m load, as shown in Fig. 13c. The test results for the VSA tracking a 15 N m load are shown in Fig. 13d, where the VSA response is smooth and almost oscillation free at large loads.

From the analysis of the above test results, it can be concluded that the VSA can quickly and accurately achieve the

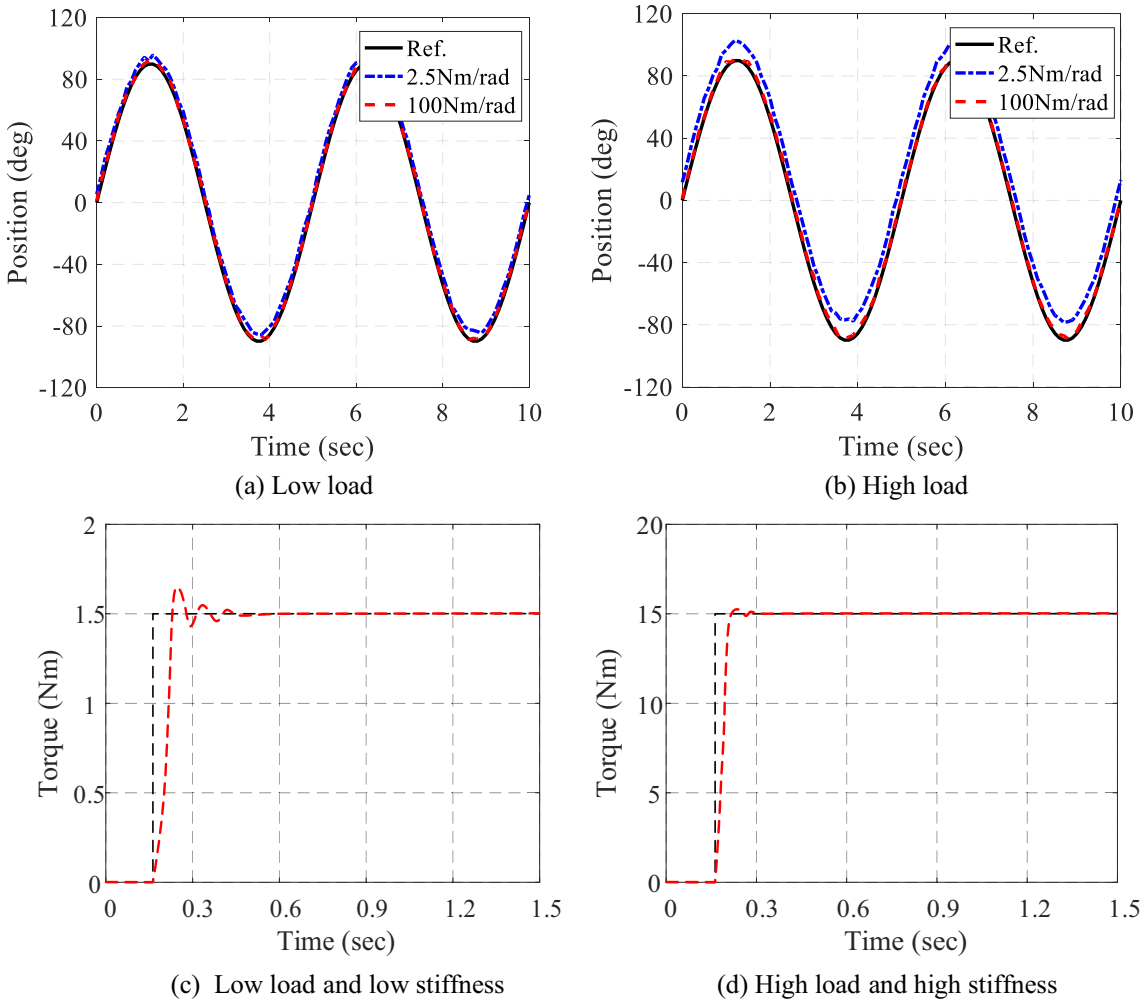

Fig. 13 2-DOF VSA position and torque response tests for different loads

torque requirements for different interaction tasks, regardless of whether the interaction load is large or small. At the same time, the VSA response does not oscillate during interaction with large loads, maintaining high response smoothness and controlling bandwidth performance.

4.5 Collision Experiments

To illustrate the physical human interaction performance of the 2-DOF VSA during an accidental active collision, a kicking-ball experiment was carried out. The length of the output link is 500 mm, which is connected to the output rod of the 2-DOF VSA, as shown in Fig. 14a. A steel ball with a diameter of 25 mm and a mass of 65 g is used. The ball is kicked and thrown out at a height of 130 mm. To eliminate the effect of the gravitational potential energy of the output rod in the relationship between the stiffness value and the distance the ball was kicked, a method controlling a single control variable was used to rotate the output rod at the same free horizontal position at a speed of 2.6 rad/s at different stiffness values. The red diamond symbol indicates the travel distance of the steel ball when being kicked at the corresponding stiffness value, as shown in Fig. 14b. The stiffness 147 N·m/rad of the VSA, the ball will travel 452 mm and the stiffness 2.5 N·m/rad of the VSA, the ball will travel 361 mm. In this experiment, the distance the ball travels at lower stiffnesses is mainly influenced by the gravitational potential energy of the rod. However, the stiffness value and the distance traveled are exponentially increasing. This also proves that the variable stiffness actuator has a good energy storage performance (ignoring the effect of gravitational potential energy). The experiment results show that the acceleration of the steel ball after a collision is affected by the different degrees of stiffness. A lower stiffness results in less elastic potential energy of the 2-DOF VSA, which is converted into the kinetic energy of the ball. The acceleration of the ball is smaller, which means that physical human interaction collisions with less stiffness are safer.

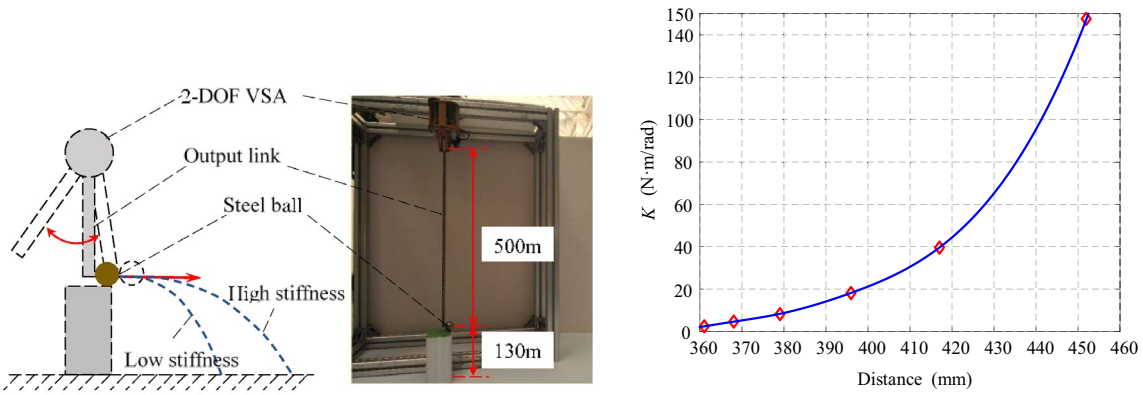

Fig. 14 Experimental setup for kicking-ball experiments. **a** An output link is attached to the 2-DOF VSA and the link kicks the steel ball (65 g, ϕ 25 mm). **b** The distance that the steel ball is kicked traveling at different stiffnesses

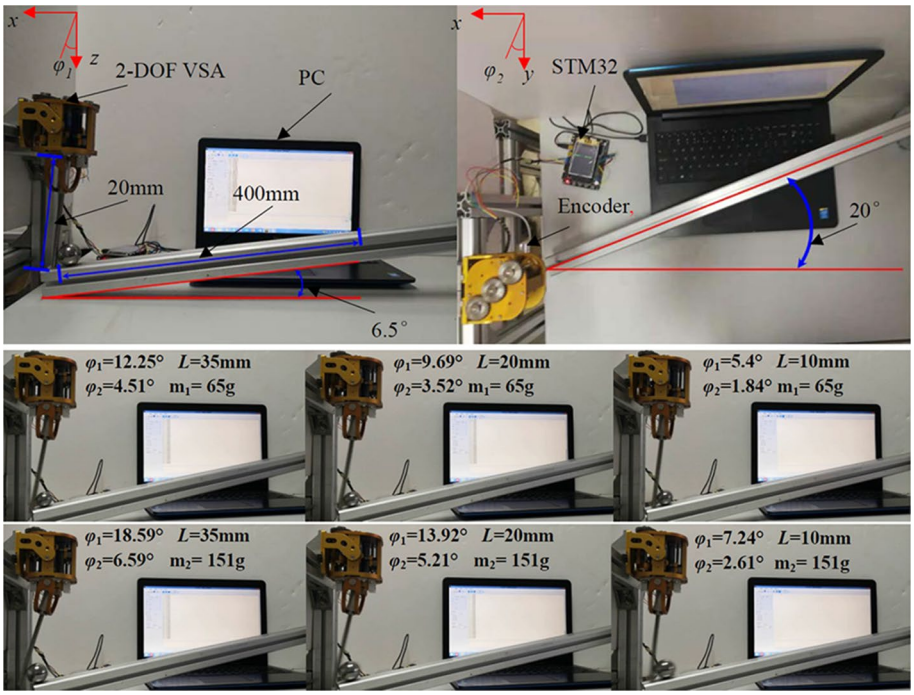

Fig. 15 Deflection angle in the direction of two degrees of freedom

As shown in Fig. 15, a passive safety collision for the physical human interaction performance test platform of 2-DOF VSA is built, which is mainly composed of actuator, STM32, encoder, guide rail, and upper computer. The inclination angle between the guide rail and the horizontal plane is 6.5°, the counterclockwise deflection is 20°, the mass of the steel ball is $m_1 = 65$ g and $m_2 = 151$ g, the stroke of the steel ball in the guide rail is 400 mm, and the length of the output rod is 20 mm. Release the steel ball with different mass to impact the actuator with 2-DOF and variable stiffness, and verify its safety collision performance in the direction of 2-DOF. Release two steel balls with the same material quality at the initial point, and adjust the variable stiffness adjusting motor, so that the effective length L of the leaf spring is 35 mm, 20 mm, and 10 mm. The deflection angle of the output rod in the direction of 2-DOF is recorded by two encoders. By recording the angle in Fig. 15, it is found that as the stiffness of the actuator increases, the passive deflection angle in the direction of 2-DOF decreases gradually, which verifies variable stiffness characteristics of the 2-DOF VSA and excellent collision energy storage characteristics.

5 Discussion

The innovation of the proposed VSA is the variable stiffness of the 2-DOF based on the parallel SWPM. The SWPM and VSU couple the 2-DOF VSA, which significantly reduces

the overall structure size and lightens the weight. The variable stiffness actuator of this study can achieve a wide range of rotation, and the stiffness adjustment range is close to zero to ∞ (Stiffness will simply approach zero in the limit, but never get there). The core part of the VSA is the uniform arrangement of the leaf springs and the single motor that can adjust the actuator stiffness. This approach both reduces motor space occupation and achieves continuity of stiffness adjustment.

In addition, compared to other types of VSAs, the actuator can provide a large range of motion (±180°) when coupled with the joint position adjustment motor. These features allow the actuator to meet most of the requirements of the physical human interaction applications, as shown in Table 1. Since the 2-DOF VSA uses a single motor to adjust the stiffness, this reduces the complexity of the control strategy. Therefore, with a simple PD feedback controller, we can obtain good position and stiffness tracking performance. The energy storage capacity is only influenced by the intrinsic leaf spring stiffness, the lever length ratio, and the deflection angle, because the leaf spring deformation is limited to the rollers, which restrict the deformation of the leaf spring in the horizontal direction. Therefore, a large deflection angle means a high energy storage capacity (4.4 J) when the spring stiffness and lever length ratio are constant. Considering the maximum load on the gear reducer, the 2-DOF VSA has a maximum torque limit of 60 N·m. In future work, the main motor and its gear reducer will be replaced to meet the torque and speed requirements for specific tasks.

The structure and performance of the humanoid robot shoulder joint directly determines the mobility, manipulation, and load-carrying performance of the upper limb of the humanoid robot. The structure of the human shoulder joint is a typical ball-and-socket joint, and the drive form is a parallel drive of muscle clusters [23, 24]. The ball-and-socket joint is a typical less-degree-of-freedom spherical wrist parallel mechanism with a structure, motion state, and properties much like those of a human joint, making it ideally suited as a prototype mechanism for the shoulder joint of a humanoid robot. A typical 3-DOF spherical manipulator or wrist provides human-like 3-D rotation, but in most robotic applications, rotation about the symmetry axis of the end-effector is not necessary and 2-D rotation alone is sufficient [25].

The high flexibility of human activity is the result of joint action of single degree of freedom and multi-degree of freedom joint, whether it is the arm or the lower limb. We are inspired by the high flexibility of the shoulder joint due to its multiple degrees of freedom. Our 2-DOF VSA is not a simple imitation of the human shoulder joint movement and behavior, but to extract the human shoulder joint multi-degree of freedom and variable stiffness of the common, using mechanical structure to achieve variable stiffness actuator of multiple degrees of freedom variable stiffness output, as shown in Table 2. A 2-DOF VSA is designed to be used together with the single degree of freedom variable stiffness joint, which not only ensures the safety of human–computer interaction, but also makes the whole robotic manipulator more flexible.

There are several methodological issues that need to be noted. In the presented design, the stiffness of the two rotation axes is adjusted by one motor. It means that the stiffness of these two rotation axes is the same at any time, and the stiffness cannot be set to different values for these two axes. If the stiffness can be set to different values in the two axis directions, this will be a design that imitates the shoulder/wrist joint. At the same time, we have carefully considered that controlling the stiffness of two rotating shafts at the same time may require multiple motors to achieve. From a control perspective, other advanced control strategies, such as neural network control [26], and model predictive control [27], can be used to deal with handling the modeling uncertainty and frictions. These factors will be considered for the improvement of the 2-DOF VSA design and control in the future work.

Table 2 Some parameters of the human shoulder joint

Name	Degree of freedom	Range of motion/(°)	Range of maximum torque/(N·m)	Range of stiffness/(N·m/rad)
Shoulder joint	3	0–125	50 ± 8	10–300
2-DOF VSA	2	0–180	60	1.54–∞

Table 1 Compared with the current series VSAs

Type	Name	DOF	Stiffness (N·m/rad)	Torque (N·m)	Size (mm)	Energy (J)	Mass (kg)
Equilibrium	FSJ [16]	1	54–826	67	119 × 92	5.3	1.41
	VS-joint [21]	1	252–3648	30	146 × 144	/	4.95
Antagonistic	QA-joint [22]	1	20–750	40	/	2.7	1.2
	SPVSA [10]	1	5.61–∞	25	82 × 70	1.4	0.48
Mechanical structure	AwAS [11]	1	30–1300	80	270 × 130	3.5	1.8
	HVSA [14]	1	4–126	1.8	100 × 100	0.86	36
	2-DOF VSA	2	1.54–∞	60	130 × 83	4.4	0.89

6 Conclusions

In this paper, a highly integrated 2-DOF VSA is proposed, which can be used for bionic multi-DOF joints. Based on the 2-DOF orthogonal motions generated by the SWPM, the stiffness adjustment of 2-DOF could be achieved by a single motor, which varies the effective lengths of the leaf springs distributed uniformly in the variable stiffness mechanism. The equilibrium position and stiffness of the actuator are independently controllable in 2-DOF. The model accuracy and prototype performance are demonstrated by regulation, tracking, and safety collision experiments, and the fidelity of the 2-DOF VSA is verified by real output torque comparison experiments. The aim of this study is to meet the deficiency of the use of single DOF variable stiffness actuators in multi-DOF humanoid robot joints like shoulder, wrist, hip, and ankle. Future studies will focus on the development of advanced control strategies to further improve the control performance of 2-DOF VSA. The actuator also could be applied to the pHRI, such as in rehabilitation medical robots and service robots.

Acknowledgements This work was supported by the National Key R&D Program of China (2018YFB1304600), National Natural Science Foundation of China (51605474, 61821005), Key Research Program of Frontier Sciences, CAS, Grant no. ZDBS-LY-JSC011, and Liaoning Revitalization Talents Program (XLYC1807090).

Availability of data and materials The data and materials that support the findings of this study are available from the corresponding author upon reasonable request.

Declarations

Conflict of interest The authors declare that they have no conflict of interest.

References

1. Ham, R. V., Sugar, T., Vanderborght, B., Hollander, K., & Lefeber, D. (2009). Compliant actuator designs. *IEEE Robotics & Automation Magazine, 3*(16), 81–94.
2. Tagliamonte, N. L., Sergi, F., Accoto, D., Carpino, G., & Guglielmelli, E. (2012). Double actuation architectures for rendering variable impedance in compliant robots: A review. *Mechatronics, 22*(8), 1187–1203.
3. Villegas, D., Van Damme, M., Vanderborght, B., Beyl, P., & Lefeber, D. (2012). Third-generation pleated pneumatic artificial muscles for robotic applications: Development and comparison with McKibben muscle. *Advanced Robotics, 26*(11–12), 1205–1227.
4. Kong, K., Bae, J., & Tomizuka, M. (2009). Control of rotary series elastic actuator for ideal force-mode actuation in human–robot interaction applications. *IEEE/ASME Transactions on Mechatronics, 14*(1), 105–118.
5. Visser, L. C., Carloni, R., & Stramigioli, S. (2011). Energy-efficient variable stiffness actuators. *IEEE Transactions on Robotics, 27*(5), 865–875.
6. Hogan, N. (1984). Adaptive control of mechanical impedance by coactivation of antagonist muscles. *IEEE Transactions on Automatic Control, 29*(8), 681–690.
7. Ménard, T., Grioli, G., & Bicchi, A. (2014). A stiffness estimator for agonistic–antagonistic variable-stiffness-actuator devices. *IEEE Transactions on Robotics, 30*(5), 1269–1278.
8. Liu, Y. W., Liu, X. G., Yuan, Z. Q., & Liu, J. G. (2019). Design and analysis of spring parallel variable stiffness actuator based on antagonistic principle. *Mechanism and Machine Theory, 140*, 44–58.
9. Tonietti, G., Schiavi, R., & Bicchi, A. (2005). Design and control of a variable stiffness actuator for safe and fast physical human/robot interaction. In *IEEE international conference on robotics and automation, Barcelona, Spain* (pp. 526–531)
10. Schiavi, R., Grioli, G., Sen, S., & Bicchi, A. (2008). VSA-II: A novel prototype of variable stiffness actuator for safe and performing robots interacting with humans. In *IEEE international conference on robotics and automation, Pasadena, USA* (pp. 2171–2176)
11. Jafari, A., Tsagarakis, N. G., & Caldwell, D. G. (2011). A novel intrinsically energy efficient actuator with adjustable stiffness (AwAS). *IEEE/ASME Transactions on Mechatronics, 18*(1), 355–365.
12. Jafari, A., Tsagarakis, N. G., Sardellitti, I., & Caldwell, D. G. (2012). A new actuator with adjustable stiffness based on a variable ratio lever mechanism. *IEEE/ASME Transactions on Mechatronics, 19*(1), 55–63.
13. Sun, J. T., Guo, Z., Zhang, Y. B., Xiao, X. H., & Tan, J. R. (2018). A novel design of serial variable stiffness actuator based on an archimedean spiral relocation mechanism. *IEEE/ASME Transactions on Mechatronics, 23*(5), 2121–2131.
14. Kim, B. S., & Song, J. B. (2012). Design and control of a variable stiffness actuator based on adjustable moment arm. *IEEE Transactions on Robotics, 28*(5), 1145–1151.
15. Groothuis, S. S., Rusticelli, G., Zucchelli, A., Stramigioli, S., & Carloni, R. (2013). The variable stiffness actuator vsaUT-II: Mechanical design, modeling, and identification. *IEEE/ASME Transactions on Mechatronics, 19*(2), 589–597.
16. Wolf, S., Eiberger, O., & Hirzinger, G. (2011). The DLR FSJ: Energy based design of a variable stiffness joint. In *IEEE international conference on robotics and automation, Shanghai, China* (pp. 5082–5089)
17. Sun, J. T., Guo, Z., Sun, D. Y., He, S. Y., & Xiao, X. H. (2018). Design, modeling and control of a novel compact, energy-efficient, and rotational serial variable stiffness actuator (SVSA-II). *Mechanism and Machine Theory, 130*, 123–136.
18. Li, J., Ma, K., & Wu, Z. (2022). Tracking control via switching and learning for a class of uncertain flexible joint robots with variable stiffness actuators. *Neurocomputing, 469*, 130–137.
19. Lindenmann, A., Heyden, E., Mas, V., Krause, D., & Matthiesen, S. (2022). Influence of friction bearings on the frequency response of a variable stiffness mechanism. *Mechanism and Machine Theory, 168*, 104588.

20. Liu, L., Leonhardt, S., Ngo, C., & Misgeld, B. J. (2019). Impedance-controlled variable stiffness actuator for lower limb robot applications. *IEEE Transactions on Automation Science and Engineering, 17*(2), 991–1004.
21. Wolf, S., & Hirzinger, G. (2008). A new variable stiffness design: Matching requirements of the next robot generation. In: *IEEE international conference on robotics and automation, Pasadena, USA* (pp. 1741–1746)
22. Eiberger, O., Haddadin, S., Weis, M., Albu-Schäffer, A., & Hirzinger, G. (2010). On joint design with intrinsic variable compliance: Derivation of the DLR QA-joint. In *IEEE international conference on robotics and automation, Anchorage, USA* (pp. 1687–1694)
23. Zheng, M., Qian, Z., Zou, Z., Peach, C., Akrami, M., & Ren, L. (2020). Subject-specific finite element modelling of the human shoulder complex part 1: model construction and quasi-static abduction simulation. *Journal of Bionic Engineering, 17*(6), 1224–1238.
24. Laribi, M. A., Ceccarelli, M., Sandoval, J., Bottin, M., & Rosati, G. (2022). Experimental validation of light cable-driven elbow-assisting device L-CADEL design. *Journal of Bionic Engineering*, *19*(2), 416–428.
25. Shang, W. S., Cong, S., Zhang, Y. X., & Liang, Y. Y. (2008). Active joint synchronization control for a 2-DOF redundantly actuated parallel manipulator. *IEEE Transactions on Control Systems Technology, 17*(2), 416–423.
26. Zhang, D. B., Hu, D. W., Shen, L. C., & Xie, H. B. (2006). A bionic neural network for fish-robot locomotion. *Journal of Bionic Engineering, 3*(4), 187–194.
27. Wang, L. K., Chen, C. F., Li, Z. Y., Dong, W., Du, Z. J., Shen, Y., & Zhao, G. Y. (2018). High precision data-driven force control of compact elastic module for a lower extremity augmentation device. *Journal of Bionic Engineering, 15*(5), 805–819.